

Long-range azimuthal correlations for partially coherent pion emission in proton-proton collisions

Peng Ru^{1,2,3,*} and Wei-Ning Zhang^{3,4,†}

¹*Institute of Quantum Matter and School of Physics and Telecommunication Engineering,
South China Normal University, Guangzhou 510006, China*

²*Key Laboratory of Quark & Lepton Physics (MOE) and Institute of Particle Physics,
Central China Normal University, Wuhan 430079, China*

³*School of Physics, Dalian University of Technology, Dalian, Liaoning 116024, China*

⁴*Department of Physics, Harbin Institute of Technology, Harbin, Heilongjiang 150006, China*

In this paper, we investigate the influence of coherent pion emission on long-range azimuthal correlations in relativistic proton-proton collisions. We study the pion momentum distribution for a coherent source with both transverse and Bjorken longitudinal expansions, and calculate the two-particle correlation function $C(\Delta\eta, \Delta\phi)$. A "ridge" structure is observed in the correlation function $C(\Delta\eta, \Delta\phi)$ of the coherent pion emission, whether the coherent source is expanding or static. The onset of this long-range azimuthal correlation can be traced back to the asymmetric initial transverse profile of the coherent source, owing to the interference in coherent emission. We further construct a partially coherent pion-emitting source by incorporating a chaotic emission component. From the experimental data of the two-pion Hanbury-Brown-Twiss correlations in pp collisions at $\sqrt{s} = 7$ TeV, we extract a coherent fraction of pion emission, which increases with increasing charged-particle multiplicity, as an input of the partially coherent source model. The ridge structure is observed in the correlation function $C(\Delta\eta, \Delta\phi)$ for the partially coherent source. The correlation becomes stronger at higher multiplicities because of the larger degrees of coherence. The results in this work are meaningful for fully understanding the collectivity in the small system of pp collisions.

PACS numbers: 25.75.Gz, 25.75.Ld, 25.75.Dw

I. INTRODUCTION

Collectivity is an important issue in high-energy nuclear physics, about which the long-range, near-side enhancement in the two-particle angular correlation function is one of the iconic phenomena. Such a "ridge" structure was first observed in relativistic nucleus-nucleus (AA) collisions [1–4], and is widely regarded as a product of the collective dynamics of the created hot/dense quantum chromodynamic (QCD) system [5–14]. However, a similar phenomenon later observed in high-multiplicity proton-nucleus (pA) and proton-proton (pp) collisions has aroused new discussions on the origin of the collectivity in such small systems [15–23]. Theoretical progress based on various mechanisms involving initial- and final-state physics has been made [24–39]. However, much work remains to be done to fully understand the collectivity in the small systems.

Hanbury-Brown-Twiss (HBT) interferometry of identical bosons (e.g., pions) can provide insight into the geometry and coherence of particle emission in high-energy nuclear and hadronic collisions [40–43]. As is well known, HBT correlations arise in a chaotic (incoherent) particle emission and will be suppressed with the presence of coherence in particle emission [44–49]. This is valuable for tracing the origin of collectivity. In a previous work [50], it was shown that the particle elliptic anisotropy, v_2 , can be generated separately in chaotic and coherent emissions in different mechanisms. In chaotic emission, as in a hydrodynamical model, v_2 can be developed

in the collective expansion of the particle source, whereas in coherent emission it is established through the interference effect [50], and is primarily a quantum-mechanical response to the source configuration [51, 52].

It is noteworthy that a significant suppression of two-pion HBT correlation strength was recently observed in small systems [53–57], indicating that there is probably a substantial coherent fraction in the pion emission in such an environment [58]. Compared to AA collisions, the effect of coherence may survive more easily in pA and pp collisions due to the less important hot-medium surroundings. Therefore, it will be interesting to see whether the long-range azimuthal correlations can exist in coherent particle emission, and how this effect will influence the collectivity in small systems.

In this paper, we investigate the influence of coherent pion emission on the long-range azimuthal correlations in relativistic pp collisions. We study the pion momentum distribution for a coherent source with both transverse and longitudinal expansions, and calculate the two-particle correlation function $C(\Delta\eta, \Delta\phi)$. We observe a ridge structure in the correlation function $C(\Delta\eta, \Delta\phi)$. We further construct a partially coherent pion-emitting source by incorporating the coherent source and a chaotic emission source described with the blast-wave model. From the ATLAS data of the two-pion HBT correlations in pp collisions at $\sqrt{s} = 7$ TeV, we extract a coherent fraction of pion emission as an input of the partially coherent source model. We find that the long-range azimuthal correlation for the partially coherent source becomes stronger with increasing multiplicity.

The rest of this paper is organized as follows. In Sec. II, we study the long-range azimuthal correlations for coherent pion emission. We review the general expressions of the pion momentum distribution of coherent emission and formulate the

*Electronic address: p.ru@m.scnu.edu.cn, pengru@mail.dlut.edu.cn

†Electronic address: wnzhang@dlut.edu.cn

coherent pion-emitting source with both transverse and longitudinal expansions. We then calculate the two-particle correlation function. In Sec. III, we focus on the partially coherent emission of pion in pp collisions at $\sqrt{s} = 7$ TeV. We extract the coherent fraction in pion emission from the experimental data of HBT correlations and discuss the results of the partially coherent source model. Finally we give a summary and discussion in Sec. IV.

II. LONG-RANGE AZIMUTHAL CORRELATIONS FOR COHERENT PION EMISSION

A. Pion momentum distribution for coherent emission

The radiation field of a classical source (current), as is well known, is a perfectly coherent multi-particle system [40, 59–62]. In this scenario, the final state of the pion field produced by a classical source $\rho(X) \equiv \rho(t, \mathbf{r})$ is a coherent state written as [40]

$$|\phi_\pi\rangle = e^{-\bar{n}/2} \exp\left(i \int d^3p \mathcal{A}(\mathbf{p}) a^\dagger(\mathbf{p})\right) |0\rangle, \quad (1)$$

where $a^\dagger(\mathbf{p})$ is the pion creation operator for momentum \mathbf{p} , and $\mathcal{A}(\mathbf{p})$ can be interpreted as the amplitude for the classical source to emit a pion with momentum \mathbf{p} [63] expressed with the on-shell ($E_p^2 = \mathbf{p}^2 + m_\pi^2$) Fourier transform of $\rho(X)$ as

$$\mathcal{A}(\mathbf{p}) = A(\mathbf{p}) \int d^4X e^{i(E_p t - \mathbf{p} \cdot \mathbf{r})} \rho(t, \mathbf{r}), \quad (2)$$

$$\text{with } A(\mathbf{p}) = [2E_p(2\pi)^3]^{-1/2} \quad (3)$$

corresponding to the pion emission amplitude of a point-like source. In addition, the pion number for the coherent state $|\phi_\pi\rangle$ obeys a Poisson distribution with a mean $\bar{n} = \int d^3p |\mathcal{A}(\mathbf{p})|^2$ [40].

The most useful property for the coherent state $|\phi_\pi\rangle$ is that it is an eigenstate of the annihilation operator, namely

$$a(\mathbf{p}) |\phi_\pi\rangle = i\mathcal{A}(\mathbf{p}) |\phi_\pi\rangle. \quad (4)$$

With this property the single-pion momentum distribution can be written as

$$P_c(\mathbf{p}) \equiv \frac{d^3\bar{n}}{d^3p} = \text{Tr}\left[D_\pi a^\dagger(\mathbf{p}) a(\mathbf{p})\right] = |\mathcal{A}(\mathbf{p})|^2, \quad (5)$$

with $D_\pi \equiv |\phi_\pi\rangle\langle\phi_\pi|$ being the density matrix of the coherent state. The amplitude $\mathcal{A}(\mathbf{p})$ expressed in Eq. (2) can be viewed as a coherent superposition of the pion-emission amplitudes at different source points [50, 63]. From this perspective, the observable $P_c(\mathbf{p})$, as the square of the absolute value of $\mathcal{A}(\mathbf{p})$, is linked up with the space-time geometry of the pion-emitting source $\rho(X)$ through an interference effect.

Utilizing Eq. (4), the multi-pion momentum distribution can be written as the product of the single-pion distributions,

$$\begin{aligned} P_c(\mathbf{p}_1, \dots, \mathbf{p}_m) &= \text{Tr}\left[D_\pi a^\dagger(\mathbf{p}_1) \cdots a^\dagger(\mathbf{p}_m) a(\mathbf{p}_m) \cdots a(\mathbf{p}_1)\right] \\ &= |\mathcal{A}(\mathbf{p}_1)|^2 \cdots |\mathcal{A}(\mathbf{p}_m)|^2. \end{aligned} \quad (6)$$

This factorization property underlies the absence of the HBT effect in a coherent state [61].

As a comparison, the momentum distributions for chaotic particle emissions such as thermal emissions are quite different [64]. For example, the single-particle momentum distribution of thermal emission mainly depends on the source temperature, and in part can be connected to the source geometry through a collective dynamical evolution (flow effect) rather than interference, due to the independent particle emissions at different source points [50, 63]. Moreover, the multi-particle momentum distribution for chaotic emission cannot be factorized into the product of the single-particle distributions, which gives rise to the HBT correlations.

In relativistic heavy-ion collisions and proton-proton collisions, the pion-emitting source is possibly partially coherent [58]. Since there is no interference effect between the chaotic and coherent emissions in the single-particle momentum distribution [63], the total distribution for a partially coherent pion source can be written as

$$P(\mathbf{p}) = P_c(\mathbf{p}) + P_\chi(\mathbf{p}), \quad (7)$$

where the subscripts c and χ indicate the coherent and chaotic emissions, respectively. Detailed discussions on the two- and multi-pion momentum distributions as well as the related HBT correlations for partially coherent source can be found in Refs. [45, 48, 49]. In general, the strength of HBT correlation will decrease with an increasing coherent fraction of pion emission.

B. Coherent pion-emitting source with transverse and longitudinal expansions

In the context of high-energy nuclear and hadronic collisions, it is meaningful to deliberate the relativistic expansion of the coherent pion-emitting source. In a previous work [50], the effect of the transverse expansion of the coherent source was studied. To further address observables such as long-range azimuthal correlations, it is essential to properly consider the longitudinal structure of the coherent source. In this work, we study a coherent source undergoing a Bjorken longitudinal expansion [65].

It is convenient to write the initial space-time distribution of such an evolving source in the $\mathcal{X} \equiv (\tau, x, y, \eta_s)$ representation rather than in the $X \equiv (t, \mathbf{r}) \equiv (t, x, y, z)$ one, where $\tau = \sqrt{t^2 - z^2}$ is the longitudinal proper time and $\eta_s = (1/2) \ln[(t+z)/(t-z)]$ is the space-time rapidity [65]. We consider an initial distribution of the coherent source written as

$$\begin{aligned} \rho_{\text{init}}(\mathcal{X}_0) &= \rho_{\text{init}}(\tau_0, x_0, y_0, \eta_{s0}) \\ &= \frac{(R_x R_y)^{-1}}{4\pi\Delta\eta_{s0}} \exp\left(-\frac{x_0^2}{2R_x^2} - \frac{y_0^2}{2R_y^2}\right) \text{Rect}\left(\frac{\eta_{s0}}{2\Delta\eta_{s0}}\right) \delta(\tau_0 - \tau_i), \end{aligned} \quad (8)$$

where R_x and R_y represent the sizes of the Gaussian transverse profile at an initial time τ_i . The coherent source is assumed to be initialized in a finite space-time rapidity range $[-\Delta\eta_{s0}, \Delta\eta_{s0}]$, formulated as the rectangle function.

To take into account both the transverse and longitudinal expansions, we further assume that each of the source elements has a velocity $\mathbf{v} = (v_x, v_y, v_z)$ in the source center-of-mass frame (CMF) written as [50, 66, 67]

$$\begin{aligned} v_x(X_0) &= (\cosh \eta_{s0})^{-1} \text{Sign}(x_0) \cdot a_x \left(\frac{|x_0|}{R_{x,\max}} \right)^{b_x}, \\ v_y(X_0) &= (\cosh \eta_{s0})^{-1} \text{Sign}(y_0) \cdot a_y \left(\frac{|y_0|}{R_{y,\max}} \right)^{b_y}, \\ v_z(X_0) &= \tanh \eta_{s0}, \end{aligned} \quad (9)$$

where the function $\text{Sign}(x) = \pm 1$ for positive/negative x ensuring that the source is transversely expansive. The magnitude of v_x (v_y) increases with $|x_0|$ ($|y_0|$), with the rate of increase determined by the positive parameters a_x and b_x (a_y and b_y). In the calculations, we take $R_{x,\max}/R_x = R_{y,\max}/R_y = 3$, and consider the source elements initiated from the elliptical transverse region $(x_0/R_{x,\max})^2 + (y_0/R_{y,\max})^2 < 1$. In this way, the requirement $|\mathbf{v}| < 1$ will be naturally guaranteed with the parameters a_x and b_x (a_y and b_y) appropriately chosen [50].

With the temporal distribution of each source element being Gaussian, the CMF space-time distribution of a source element (SE) initiated from X_0 , denoted $\rho_{X_0}^{\text{SE}}$, can be expediently written in the $X = (t, \mathbf{r})$ representation as $\rho_{X_0}^{\text{SE}}(X) = \tilde{\rho}_{X_0}^{\text{SE}}(X - X_0) = \tilde{\rho}_{X_0}^{\text{SE}}(t - t_0, \mathbf{r} - \mathbf{r}_0)$, with

$$\tilde{\rho}_{X_0}^{\text{SE}}(X) = \sqrt{\frac{2}{\pi}} T_s^{-1} \exp\left(-\frac{t^2}{2T_s^2}\right) \delta^{(3)}(\mathbf{r} - \mathbf{v}t), \quad (t > 0), \quad (10)$$

where the wide-tilde $\tilde{\rho}_{X_0}^{\text{SE}}(X)$ is the equivalent source-element distribution with the initial coordinate shifted from (t_0, \mathbf{r}_0) to $(0, \mathbf{0})$, and T_s is the CMF duration time of the source element [50]. By considering that all the source elements have the same longitudinal proper lifetime τ_s , we have $T_s = \tau_s \cosh \eta_{s0}$. For legibility, we supplement that $X_0 = (t_0, x_0, y_0, z_0) = (\tau_0 \cosh \eta_{s0}, x_0, y_0, \tau_0 \sinh \eta_{s0})$. Overall, $\tilde{\rho}_{X_0}^{\text{SE}}(X)$ depends on both $T_s = T_s(X_0)$ and the source element moving velocity $\mathbf{v} = \mathbf{v}(X_0)$ in the form of Eq. (9).

Assuming that all the source elements are evolved from the initial source $\rho_{\text{init}}(X_0)$, one can finally write the space-time distribution of the expanding coherent source in the CMF by integrating all the sub-distributions $\rho_{X_0}^{\text{SE}}(X)$ together as

$$\rho(X) = \int d^4 X_0 \rho_{\text{init}}(X_0) \rho_{X_0}^{\text{SE}}(X), \quad (11)$$

where $\int d^4 X_0 \equiv \int d\tau_0 dx_0 dy_0 d\eta_{s0}$ with normalization condition $\int d^4 X_0 \rho_{\text{init}}(X_0) = 1$. At this point, we have completed the parametrization of the coherent source with both transverse and longitudinal expansions.

The single-pion momentum distribution for the coherent source $\rho(X)$ can already be calculated utilizing Eqs. (2), (3), and (5). All the same, it is very useful to introduce the pion-emission amplitude of the sub-source $\rho_{X_0}^{\text{SE}}(X)$ [50], expressed as

$$\mathcal{A}_c^{\text{SE}}(X_0, \mathbf{p}) \equiv A_c(\mathbf{p}) G_0\{[p \cdot u(X_0)](\gamma_u^{-1} T_s)\}$$

$$\begin{aligned} &= A_c(\mathbf{p}) \int d^4 X e^{ip \cdot X} \tilde{\rho}_{X_0}^{\text{SE}}(X) \\ &= [2E_p(2\pi)^3]^{-\frac{1}{2}} \int_0^\infty dt \sqrt{\frac{2}{\pi}} \exp\left[it([p \cdot u(X_0)](\gamma_u^{-1} T_s)) - \frac{t^2}{2}\right], \end{aligned} \quad (12)$$

where $A_c(\mathbf{p})$ is in the form of Eq. (3), the function G_0 is the Fourier transform of the sub-distribution $\tilde{\rho}_{X_0}^{\text{SE}}(X)$, and $u(X_0) = \gamma_u(1, \mathbf{v}(X_0))$ is the source element 4-velocity, with the Lorentz factor $\gamma_u = (1 - v^2)^{-1/2}$.

In this way, the Lorentz invariant pion momentum distribution for the coherent source $\rho(X)$ can be readily written as the result of the coherent superposition of all the sub-source pion-emission amplitudes [50] as

$$\begin{aligned} E_p P_c(\mathbf{p}) &= E_p \left| \int d^4 X_0 \rho_{\text{init}}(X_0) e^{ip \cdot X_0} \mathcal{A}_c^{\text{SE}}(X_0, \mathbf{p}) \right|^2 \\ &= [2(2\pi)^3]^{-1} \left| \int d^4 X_0 \rho_{\text{init}}(X_0) e^{ip \cdot X_0} G_0\{[p \cdot u(X_0)](\gamma_u^{-1} T_s)\} \right|^2 \\ &= [2(2\pi)^3]^{-1} \left| \int d^4 X_0 \rho_{\text{init}}(X_0) \exp[im_T \tau_0 \cosh(y - \eta_{s0}) - i\mathbf{p}_T \cdot \mathbf{x}_{0T}] \right. \\ &\quad \left. \times G_0\{[p \cdot u(X_0)](\gamma_u^{-1} \cosh \eta_{s0} \tau_s)\} \right|^2, \end{aligned} \quad (13)$$

where $m_T = (p_T^2 + m_\pi^2)^{1/2}$ is the pion transverse mass, y the pion rapidity, and $\mathbf{x}_{0T} = (x_0, y_0)$ the transverse vector. With the role of the source expansion involved in function G_0 , Eq. (13) reveals how the momentum distribution is related to the source initial geometry featured in ρ_{init} . Equation (13) will be used in the rest of this paper to study the long-range azimuthal correlations.

C. Long-range two-particle azimuthal correlations

Next, we study the two-particle angular correlation function defined as

$$C(\Delta\eta, \Delta\phi) = \frac{S(\Delta\eta, \Delta\phi)}{B(\Delta\eta, \Delta\phi)}, \quad (14)$$

which is commonly used in the experimental measurement [17, 21]. In our theoretical calculations, to obtain the two-particle distribution $S(\Delta\eta, \Delta\phi)$, we randomly generate 10^6 pions in terms of the single-particle momentum distribution expressed as Eq. (13) and sort the pion pairs into kinematic bins defined with two-particle relative azimuthal angle $\Delta\phi \equiv \phi_1 - \phi_2$ and relative pseudo-rapidity $\Delta\eta \equiv \eta_1 - \eta_2$. Then, we similarly evaluate the "background" distribution, $B(\Delta\eta, \Delta\phi)$, by additionally imposing an azimuthal isotropy condition when randomly generating pions. Therefore, the case $C(\Delta\eta, \Delta\phi) = 1$ corresponds to a vanishing two-particle azimuthal correlation.

In panel (a) of Fig. 1, we show the two-particle angular correlation function for a coherent pion-emitting source with both transverse and longitudinal expansions. In the calculations, the initial transverse size and shape of the expanding coherent source are taken to be $R_T \equiv \sqrt{R_x R_y} = 0.12$ fm and

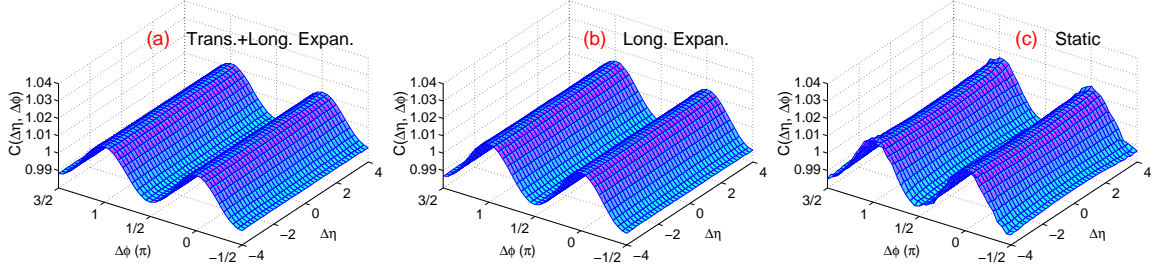


FIG. 1: (Color online) Two-particle correlation function, $C(\Delta\eta, \Delta\phi)$, for coherent pion-emitting sources, with (a) both transverse and longitudinal expansions, (b) longitudinal expansion only, and (c) no expansion (static source). In calculations, kinematic region of pion is taken to be $|\eta| < 2.5$ and $0.5 < p_T < 5.0$ GeV [17, 21].

$S_T \equiv R_y/R_x = 1.45$, respectively. For the range of the source space-time rapidity, we take $\Delta\eta_{s0} = 4$. The initial time and lifetime of the coherent source are taken to be $\tau_i = 0$ fm/c and $\tau_s = 0.5$ fm/c, respectively. In addition, we take the velocity parameters to be $a_x = 0.6$, $a_y = 0.56$ and $b_{x,y} = 0.5$ for an anisotropic transverse expansion of the coherent source [50]. To study the long-range azimuthal correlations, we pick out the pions generated in the kinematic range $|\eta| < 2.5$ and $0.5 < p_T < 5.0$ GeV [17, 21] for the calculations.

In panel (a) of Fig. 1, one can observe a remarkable double-ridge structure [20, 29] for the coherent pion emission. To trace the origin of this phenomenon, we show the results for two other typical cases, i.e., the source with longitudinal ex-

pansion only (non-expansive in transverse) and the source being static, in panels (b) and (c) of Fig. 1, respectively. The source parameters for the three cases in Fig. 1 are same, except for the expansion velocity. It is interesting to observe that the two-particle correlation functions for the three cases are very similar. This implies that, for a coherent emission, the near-side ridge structure can arise without source collective expansion, and the effect of the source expansion velocity on $C(\Delta\eta, \Delta\phi)$ is small (also checked by varying the transverse velocity and geometry). It is noteworthy that the expressions of the pion momentum distributions for the latter two cases can be simplified as

$$\begin{aligned} \frac{dN_c^3}{p_T dp_T dy d\phi} &= E_p \left| \int d\mathbf{x}_{0T} \frac{(R_x R_y)^{-1}}{2\pi} e^{i\mathbf{p}_T \cdot \mathbf{x}_{0T}} \exp\left(-\frac{x_0^2}{2R_x^2} - \frac{y_0^2}{2R_y^2}\right) \int d\tau_0 \int_{-\Delta\eta_{s0}}^{+\Delta\eta_{s0}} d\eta_{s0} \frac{\delta(\tau_0 - \tau_i)}{2\Delta\eta_{s0}} e^{im_T \tau_0 \cosh(y - \eta_{s0})} \mathcal{A}_c^{\text{SE}}(\mathbf{X}_0, \mathbf{p}) \right|^2 \\ &= \frac{(2\pi)^{-3}}{2(2\Delta\eta_{s0})^2} \exp\left\{-p_T^2 \left[(R_x \cos \phi)^2 + (R_y \sin \phi)^2\right]\right\} \left| \int_{-\Delta\eta_{s0}}^{+\Delta\eta_{s0}} d\eta_{s0} e^{im_T \tau_i \cosh(y - \eta_{s0})} G_0(m_T \cosh(y - \eta_{s0}) \tau_s) \right|^2, \end{aligned} \quad (\text{longitudinally expansive}). \quad (15)$$

$$\frac{dN_c^3}{p_T dp_T dy d\phi} = \frac{(2\pi)^{-3}}{2} \exp\left\{-p_T^2 \left[(R_x \cos \phi)^2 + (R_y \sin \phi)^2\right]\right\} \left| G_0(m_T \cosh y \tau_s) \right|^2, \quad (\text{static source, } \tau_i = 0 \text{ fm/c}). \quad (16)$$

Clearly, Eqs. (15) and (16) share the same elliptical-type azimuthal angle component $e^{-p_T^2 [(R_x \cos \phi)^2 + (R_y \sin \phi)^2]}$, which is independent of the rapidity. This factorization property is responsible for the strong long-range correlations arising with the asymmetric transverse profile, i.e., $R_x \neq R_y$. As discussed in Secs. II A and II B, this long-range azimuthal anisotropy is connected to the source geometry through the interference in coherent emission.

To further study the effect of the source expansion on the coherent emission, we plot in Fig. 2 the pion rapidity (left-hand panel) and transverse momentum (right-hand panel) distributions for the three typical cases. One can see that the Bjorken longitudinal expansion of the coherent source has a

significant impact on the rapidity distribution, and a visible effect on the p_T distribution. However, the effects of the transverse expansion on both rapidity and transverse momentum distributions are rather weak. This distinction is related to the asymmetry between the transverse and longitudinal source structures. In this sense, equation (15) virtually serves as an approximation for the general case involving both transverse and longitudinal source expansions, expressed as Eq. (13).

The results presented in this section are consistent with the finding in our previous work [50], where the effects of the transverse expansion of coherent source on the p_T spectrum and v_2 are shown to be largely reduced owing to the interference in coherent emission. In contrast, the transverse expan-

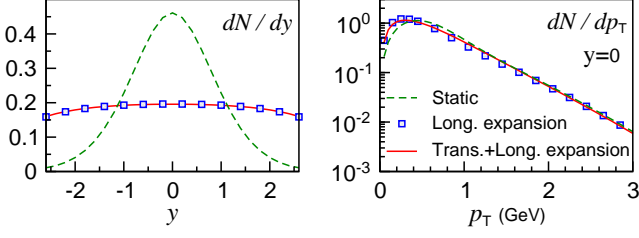


FIG. 2: (Color online) Normalized pion rapidity distribution (left-hand panel) and transverse momentum distribution at central rapidity (right-hand panel) for coherent sources with both transverse and longitudinal expansions, with longitudinal expansion only, and without expansion (static source), corresponding to the results in Fig. 1.

sion of chaotic source has considerable flow effects [50].

To summarize, the long-range azimuthal correlations for the expanding coherent source are to a large extent related to the initial transverse profile of the source (i.e., R_x and R_y).

III. PARTIALLY COHERENT PION EMISSION IN PROTON-PROTON COLLISIONS

A. Chaotic component in partially coherent emission

In this subsection, we begin to focus on the long-range azimuthal correlations and the related phenomena in pp collisions. In relativistic pp collisions, e.g., at the LHC, the created pion-emitting source is possibly partially coherent [53–57], and there should be a chaotic component in the pion emission. To characterize the chaotic pion emission, we utilize the widely used blast-wave (BW) spectrum [68, 69] as follows:

$$\frac{dN_\chi^3}{p_T dp_T dy d\phi} \propto \int_0^R r dr m_T I_0 \left(\frac{p_T \sinh \rho}{T} \right) K_1 \left(\frac{m_T \cosh \rho}{T} \right), \quad (17)$$

where I_0 and K_1 are the modified Bessel functions, T is the freeze-out temperature, R is the source radius, and ρ is the transverse velocity profile given by

$$\rho = \tanh^{-1} [(r/R)^n \beta_s], \quad (18)$$

with β_s being the transverse expansion velocity at the surface.

In Fig. 3 we show the pion transverse momentum distribution for the chaotic emission. In the calculations, we take $T = 100$ MeV and $n = 2$, and vary the velocity β_s to study the effect of the transverse expansion of the chaotic source [68, 69]. Obviously, the p_T distribution becomes “harder” (wider) with increasing transverse expansion velocity, which is expected and is also referred to as the radial flow effect.

With the given momentum distributions for both coherent and chaotic emissions [Eqs. (13) and (17)] and their proportions in pion emission, the total distribution for a partially coherent source can be evaluated by using Eq. (7). It is noted that the single-particle momentum distribution for chaotic emission expressed in Eq. (17) is homogeneous for both rapidity and azimuthal angle components. Thus, in this partially coherent pion emission model, the long-range azimuthal correlation will be entirely from the coherent emission part.

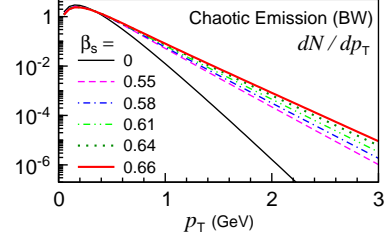


FIG. 3: (Color online) Normalized pion transverse momentum distribution for chaotic emission in blast-wave model. Parameter β_s for transverse expansion velocity of the chaotic source is taken to be 0, 0.55, 0.58, 0.61, 0.64, and 0.66.

B. Extracting coherent fraction from two-pion HBT measurement

To complete the partially coherent source model, it is necessary to appropriately estimate the fraction of coherent/chaotic emission in the total pion momentum distribution. As is discussed in Sec. II A, the pion HBT correlations can provide an excellent probe of the degree of coherence in pion emission. For example, the strength parameter λ^{HBT} for the two-pion HBT correlations, also called the chaoticity parameter, will decrease with increasing degree of coherence in pion emission. Based on this, we extract the coherent fraction of pion emission, f_c , as a function of the charged-particle multiplicity N_{ch} from the measurement of λ^{HBT} in pp collisions at $\sqrt{s} = 7$ TeV performed by ATLAS [55], which is shown in Fig. 4.

We note that the experimentalists have made numerous efforts to effectively exclude the final-state effects [55], e.g.,

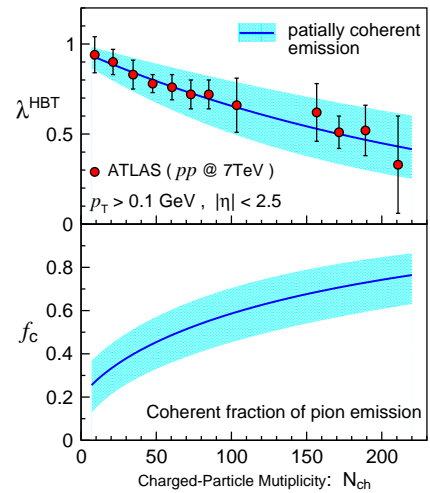


FIG. 4: (Color online) Strength parameter λ^{HBT} of two-pion HBT correlation in pp collisions at $\sqrt{s} = 7$ TeV as a function of charged-particle multiplicity (top panel) and extracted coherent fraction of pion emission (bottom panel). In top panel, red disc represents ATLAS data [55], blue curve is fitted value with parametrization form $\lambda^{\text{HBT}}(N_{\text{ch}}) = \gamma e^{-N_{\text{ch}}^\delta}$, and shaded area corresponds to a likelihood band.

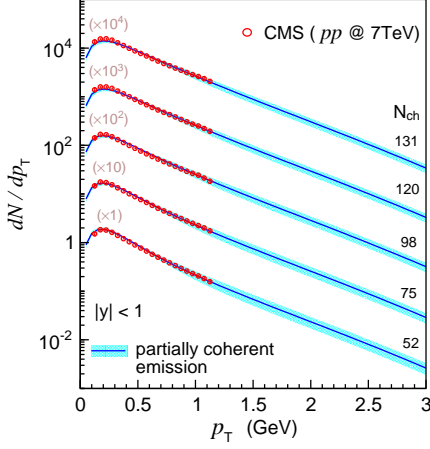


FIG. 5: (Color online) Normalized transverse momentum distribution of pion for five multiplicity classes in pp collisions at $\sqrt{s} = 7$ TeV. Blue curve represents result of partially coherent emission, with shaded area corresponding to band of extracted f_c in Fig. 4. CMS data [75] are shown as a red circle.

the long-range Coulomb force, which may affect the measurement of λ^{HBT} . Therefore, we assume that the measured λ^{HBT} suppression ($\lambda^{\text{HBT}} < 1$) is to a large extent related to the presence of coherence in pion emission. In the top panel of Fig. 4, the solid curve corresponds to the fitted values with the parametrization form $\lambda^{\text{HBT}}(N_{\text{ch}}) = \gamma e^{-N_{\text{ch}}\delta}$ [55]. To address other effects that may smear the signal of coherence [70–72], we consider additionally a likelihood band around the fitted values shown as the shaded area.

With the extracted $\lambda^{\text{HBT}}(N_{\text{ch}})$, one can estimate the coherent fraction in pion emission using the following relation [40, 45]:

$$f_c(N_{\text{ch}}) \approx [1 - \lambda^{\text{HBT}}(N_{\text{ch}})]^{1/2}. \quad (19)$$

The obtained $f_c(N_{\text{ch}})$, to be used as an input of the partially coherent pion emission model, is shown in the bottom panel of Fig. 4, with the shaded area corresponding to the band of the extracted $\lambda^{\text{HBT}}(N_{\text{ch}})$. It is interesting to see that the degree of coherence increases with N_{ch} , which may indicate that the coherence is more likely to arise from the state with a higher density of particle occupation [73, 74]. The underlying mechanism can be studied in future. We note that a similar multiplicity dependence for the HBT correlation strengths has been observed in the other experiments at the LHC [53–57].

C. Results of partially coherent source

Next, we present the results of the partially coherent pion-emitting source for pp collisions at $\sqrt{s} = 7$ TeV.

Figure 5 shows the results for pion transverse momentum distribution, in which the shaded areas correspond to the bands of the extracted f_c as shown in Fig. 4. One can see that the results with the partially coherent pion emission model can well describe the CMS data [75] in the five multiplicity classes.

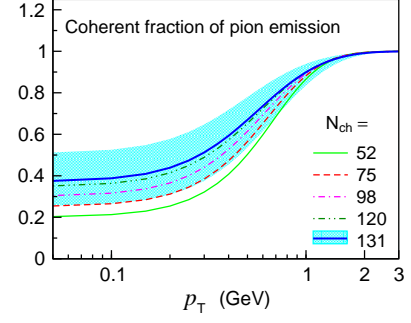


FIG. 6: (Color online) Coherent fraction of pion emission as a function of transverse momentum, corresponding to results in Fig. 5.

In the calculations, for the coherent component, we consider a source with both longitudinal and transverse expansions with the source parameters taken the same as in Sec. II C. It is observed from the CMS data that the p_T spectrum becomes harder with increasing multiplicity [75], which may indicate a stronger radial flow effect in the chaotic emission for a higher multiplicity. Thus, we use a transverse expansion velocity (β_s) increasing with the multiplicity for the chaotic source, and take the source parameters the same as in Sec. III A (the used values of β_s are shown in Fig. 3). We do not take into account the multiplicity dependence for the transverse expansion of the coherent source due to the negligible observable effect as is discussed in Sec. II C. To further simplify the model setting, we mainly focus on the events in the intermediate-to-high-multiplicity region (e.g., $50 \lesssim N_{\text{ch}} \lesssim 130$) in this work. In total, there are two multiplicity-dependent inputs in this partially coherent pion emission model, which are the coherent fraction in pion emission (f_c) and the transverse expansion velocity of the chaotic source (β_s).

To better understand the pion transverse momentum distribution of the partially coherent emission, we plot in Fig. 6 the coherent fraction of pion emission as a function of p_T . For the multiplicity class, $N_{\text{ch}} = 131$, we also show the shaded area corresponding to the band of the extracted f_c . We ob-

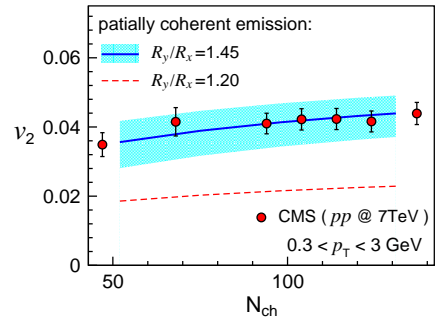


FIG. 7: (Color online) Elliptic anisotropy of pion as a function of charged-particle multiplicity in pp collisions at $\sqrt{s} = 7$ TeV. Blue solid curve is result of partially coherent emission with $S_T = 1.45$, and shaded band is from extracted f_c in Fig. 4. Red dashed curve is result with $S_T = 1.20$. Red disc represents CMS data for charged particles [20].

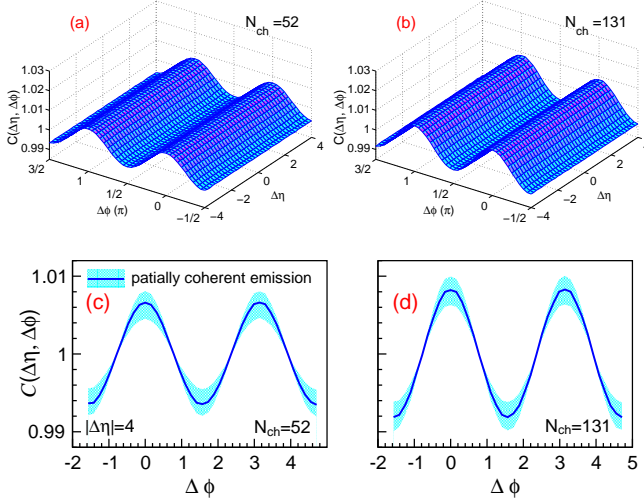


FIG. 8: (Color online) Two-particle correlation function, $C(\Delta\eta, \Delta\phi)$, for partially coherent pion-emitting sources for two multiplicity classes in pp collisions. Panels (c) and (d) show values at $|\Delta\eta| = 4$, with shaded band from extracted f_c in Fig. 4. In calculations, kinematic region of pion is taken to be $|\eta| < 2.5$ and $0.5 < p_T < 5.0$ GeV [17, 21].

serve from Fig. 6 that the coherent fraction increases with p_T , which is consistent with the experimental observation of a decreasing λ^{HBT} versus p_T [53, 55, 57].

In Fig. 7, we plot the pion elliptic anisotropy v_2 for the partially coherent emission as a function of the charged-particle multiplicity. For the blue solid curve, the source parameters are the same as above, of which the most relevant one is the initial transverse shape parameter $S_T \equiv R_y/R_x$ for the coherent source (taken to be 1.45). We also show the shaded area corresponding to the band of the extracted f_c . To illustrate the dependence on S_T for v_2 , we additionally plot the result with $S_T = 1.20$ as the red dashed curve. In general, v_2 will increase with both S_T and the coherent fraction (or N_{ch}) in our partially coherent source model. For comparison, we also show the CMS data for charged particles [20]. We can see that, with the current model, the result for $S_T = 1.45$ agrees well with the data.

At the end of this section, we calculate the two-particle angular correlation function $C(\Delta\eta, \Delta\phi)$ of the partially coherent pion emission for pp collisions with $N_{\text{ch}} = 52$ and 131, and show the results in panels (a) and (b) of Fig. 8, respectively. For better comparison, the values of $C(\Delta\eta, \Delta\phi)$ at $|\Delta\eta| = 4$ are plotted in panels (c) and (d) with the shaded bands from the extracted f_c . We observe from Fig. 8 that, with the presence of coherence in pion emission, the ridge structure can manifest itself in the $C(\Delta\eta, \Delta\phi)$, and the correlation becomes stronger for a higher multiplicity class, which corresponds to a larger coherent fraction in pion emission.

IV. SUMMARY AND DISCUSSION

In this work, we investigate the influence of coherent pion emission on the long-range azimuthal correlations in relativistic proton-proton collisions.

We study the pion momentum distribution for a coherent pion-emitting source with both transverse and longitudinal expansions, and calculate the two-particle correlation function $C(\Delta\eta, \Delta\phi)$. It is found that the function $C(\Delta\eta, \Delta\phi)$ has a remarkable ridge structure for the coherent source whether it is expanding or static. The onset of this long-range azimuthal correlation can be traced back to the asymmetric initial transverse profile of the coherent source, owing to interference in coherent emission. Because of the interference effect, the transverse expansion of the coherent source has a slight influence on the pion momentum distribution. However, the Bjorken longitudinal expansion significantly shapes the pion rapidity distribution.

To address the pion emission in pp collisions, we construct a partially coherent pion-emitting source by incorporating the coherent source and a chaotic emission source described with the blast-wave model. Using the experimental data of the two-pion HBT correlation strengths in pp collisions at $\sqrt{s} = 7$ TeV, we extract a coherent fraction of pion emission as an input of the partially coherent source model, which increases with charged-particle multiplicity. We find the results with the current model can well reproduce the experimental data of the transverse momentum spectrum and the elliptic anisotropy in the intermediate-to-high multiplicity classes. Furthermore, the ridge structure is still clear in the function $C(\Delta\eta, \Delta\phi)$ for the partially coherent emission. This long-range correlation becomes stronger with increasing multiplicity due to the increasing degree of coherence.

It should be noted that, to clarify the effect of coherent emission on the $C(\Delta\eta, \Delta\phi)$, we have taken no account of the possible emergence of the ridge correlation in the chaotic emission component in this work, which may be related to the dynamics of the collective expansion of chaotic source, and be more pronounced in higher-multiplicity events. Even so, the results in this paper indicate the importance of deliberating the possible coherent particle emission, for fully understanding the collectivity in the small systems.

Acknowledgments

P.R. would like to thank Prof. Ben-Wei Zhang for his kind invitation to visit CCNU. This research was supported in part by the National Natural Science Foundation of China under Grant No. 11675034, by the China Postdoctoral Science Foundation under Project No. 2019M652929, and by the MOE Key Laboratory of Quark and Lepton Physics (CCNU) under Project No. QLPL201802.

- 062301 (2010).
- [3] S. Chatrchyan *et al.* [CMS Collaboration], JHEP **1107**, 076 (2011).
 - [4] G. Aad *et al.* [ATLAS Collaboration], Phys. Rev. C **86**, 014907 (2012).
 - [5] P. Romatschke and U. Romatschke, Phys. Rev. Lett. **99**, 172301 (2007).
 - [6] H. Song and U. Heinz, Phys. Lett. B **658**, 279 (2008).
 - [7] B. Schenke, S. Jeon and C. Gale, Phys. Rev. Lett. **106**, 042301 (2011).
 - [8] P. Božek, Phys. Rev. C **85**, 034901 (2012).
 - [9] F. G. Gardim, F. Grassi, M. Luzum and J. Y. Ollitrault, Phys. Rev. Lett. **109**, 202302 (2012).
 - [10] C. Gale, S. Jeon, B. Schenke, P. Tribedy and R. Venugopalan, Phys. Rev. Lett. **110**, 012302 (2013).
 - [11] H. Song, S. Bass and U. Heinz, Phys. Rev. C **89**, 034919 (2014).
 - [12] L. Pang, Q. Wang and X. N. Wang, Phys. Rev. C **89**, 064910 (2014).
 - [13] L. He, T. Edmonds, Z. W. Lin, F. Liu, D. Molnar and F. Wang, Phys. Lett. B **753**, 506 (2016).
 - [14] H. Song, Y. Zhou and K. Gajdosova, Nucl. Sci. Tech. **28**, 99 (2017).
 - [15] V. Khachatryan *et al.* [CMS Collaboration], JHEP **1009**, 091 (2010).
 - [16] B. B. Abelev *et al.* [ALICE Collaboration], Phys. Lett. B **726**, 164 (2013).
 - [17] G. Aad *et al.* [ATLAS Collaboration], Phys. Rev. Lett. **116**, 172301 (2016).
 - [18] V. Khachatryan *et al.* [CMS Collaboration], Phys. Rev. Lett. **116**, 172302 (2016).
 - [19] R. Aaij *et al.* [LHCb Collaboration], Phys. Lett. B **762**, 473 (2016).
 - [20] V. Khachatryan *et al.* [CMS Collaboration], Phys. Lett. B **765**, 193 (2017).
 - [21] M. Aaboud *et al.* [ATLAS Collaboration], Phys. Rev. C **96**, 024908 (2017).
 - [22] C. Aidala *et al.* [PHENIX Collaboration], Nature Phys. **15**, 214 (2019).
 - [23] J. Adam *et al.* [STAR Collaboration], Phys. Rev. Lett. **122**, 172301 (2019).
 - [24] A. Dumitru, K. Dusling, F. Gelis, J. Jalilian-Marian, T. Lappi and R. Venugopalan, Phys. Lett. B **697**, 21 (2011).
 - [25] K. Werner, M. Bleicher, B. Guiot, I. Karpenko and T. Pierog, Phys. Rev. Lett. **112**, 232301 (2014).
 - [26] P. Bozek, W. Broniowski and G. Torrieri, Phys. Rev. Lett. **111**, 172303 (2013).
 - [27] G. L. Ma and A. Bzdak, Phys. Lett. B **739**, 209 (2014).
 - [28] A. Bzdak and G. L. Ma, Phys. Rev. Lett. **113**, 252301 (2014).
 - [29] B. Schenke, S. Schlichting, P. Tribedy and R. Venugopalan, Phys. Rev. Lett. **117**, 162301 (2016).
 - [30] R. D. Weller and P. Romatschke, Phys. Lett. B **774**, 351 (2017).
 - [31] M. Greif, C. Greiner, B. Schenke, S. Schlichting and Z. Xu, Phys. Rev. D **96**, 091504 (2017).
 - [32] C. Bierlich, G. Gustafson and L. Lönnblad, Phys. Lett. B **779**, 58 (2018).
 - [33] W. Zhao, Y. Zhou, H. Xu, W. Deng and H. Song, Phys. Lett. B **780**, 495 (2018).
 - [34] M. Mace, V. V. Skokov, P. Tribedy and R. Venugopalan, Phys. Rev. Lett. **121**, 052301 (2018).
 - [35] B. Blok and U. A. Wiedemann, Phys. Lett. B **795**, 259 (2019).
 - [36] C. Zhang, C. Marquet, G. Y. Qin, S. Y. Wei and B. W. Xiao, Phys. Rev. Lett. **122**, 172302 (2019).
 - [37] U. Heinz and J. S. Moreland, J. Phys. Conf. Ser. **1271**, 012018 (2019).
 - [38] M. Nie, L. Yi, J. Jia and G. Ma, arXiv:1906.01422 [nucl-th].
 - [39] B. Schenke, C. Shen and P. Tribedy, arXiv:1908.06212 [nucl-th].
 - [40] M. Gyulassy, S. K. Kauffmann and L. W. Wilson, Phys. Rev. C **20**, 2267 (1979).
 - [41] U. A. Wiedemann and U. Heinz, Phys. Rept. **319**, 145 (1999).
 - [42] R. M. Weiner, Phys. Rept. **327**, 249 (2000).
 - [43] M. A. Lisa, S. Pratt, R. Soltz and U. Wiedemann, Ann. Rev. Nucl. Part. Sci. **55**, 357 (2005).
 - [44] S. V. Akkelin, R. Lednicky and Y. M. Sinyukov, Phys. Rev. C **65**, 064904 (2002).
 - [45] C. Y. Wong and W. N. Zhang, Phys. Rev. C **76**, 034905 (2007).
 - [46] J. Liu, P. Ru, W. N. Zhang and C. Y. Wong, Int. J. Mod. Phys. E **22**, 1350083 (2013).
 - [47] J. Liu, P. Ru, W. N. Zhang and C. Y. Wong, J. Phys. G **41**, 125101 (2014).
 - [48] D. Gangadharan, Phys. Rev. C **92**, 014902 (2015).
 - [49] G. Bary, P. Ru and W. N. Zhang, J. Phys. G **45**, 065102 (2018).
 - [50] P. Ru, G. Bary and W. N. Zhang, Phys. Lett. B **777**, 79 (2018).
 - [51] M. H. Anderson, J. R. Ensher, M. R. Matthews, C. E. Wieman and E. A. Cornell, Science **269**, 198 (1995).
 - [52] K. B. Davis, M.-O. Mewes, M. R. Andrews, N. J. van Druten, D. S. Durfee, D. M. Kurn and W. Ketterle, Phys. Rev. Lett. **75**, 3969 (1995).
 - [53] V. Khachatryan *et al.* [CMS Collaboration], JHEP **1105**, 029 (2011).
 - [54] K. Aamodt *et al.* [ALICE Collaboration], Phys. Rev. D **84**, 112004 (2011).
 - [55] G. Aad *et al.* [ATLAS Collaboration], Eur. Phys. J. C **75**, 466 (2015).
 - [56] R. Aaij *et al.* [LHCb Collaboration], JHEP **1712**, 025 (2017).
 - [57] A. M. Sirunyan *et al.* [CMS Collaboration], Phys. Rev. C **97**, 064912 (2018).
 - [58] R. J. Glauber, Nucl. Phys. A **774**, 3 (2006).
 - [59] R. J. Glauber, Phys. Rev. **84**, 395 (1951).
 - [60] R. J. Glauber, Phys. Rev. Lett. **10**, 84 (1963).
 - [61] R. J. Glauber, Phys. Rev. **130**, 2529 (1963).
 - [62] R. J. Glauber, Phys. Rev. **131**, 2766 (1963).
 - [63] C. Y. Wong, *Introduction to High-Energy Heavy-Ion Collisions* (World Scientific, Singapore, 1994), Chapter 17.
 - [64] F. Cooper and G. Frye, Phys. Rev. D **10**, 186 (1974).
 - [65] J. D. Bjorken, Phys. Rev. D **27**, 140 (1983).
 - [66] W. N. Zhang, Y. Y. Ren and C. Y. Wong, Phys. Rev. C **74**, 024908 (2006).
 - [67] J. Yang, Y. Y. Ren and W. N. Zhang, Adv. High Energy Phys. **2015**, 846154 (2015).
 - [68] E. Schnedermann, J. Sollfrank and U. Heinz, Phys. Rev. C **48**, 2462 (1993).
 - [69] B. Abelev *et al.* [ALICE Collaboration], Phys. Rev. C **88**, 044910 (2013).
 - [70] S. Nickerson, T. Csörgo and D. Kiang, Phys. Rev. C **57**, 3251 (1998).
 - [71] W. N. Zhang, Z. T. Yang and Y. Y. Ren, Phys. Rev. C **80**, 044908 (2009).
 - [72] C. Plumberg and U. Heinz, Phys. Rev. C **98**, 034910 (2018).
 - [73] J. P. Blaizot, F. Gelis, J. F. Liao, L. McLerran and R. Venugopalan, Nucl. Phys. A **873**, 68 (2012).
 - [74] J. Berges, K. Boguslavski, M. Mace and J. M. Pawłowski, arXiv:1909.06147 [hep-ph].
 - [75] S. Chatrchyan *et al.* [CMS Collaboration], Eur. Phys. J. C **72**, 2164 (2012).